Research Paper

Structure and variations of global planetary boundary layer top from 2008-2022 multiple GNSS RO observations

Huihuang Xing [a], Shuanggen Jin [a,b,c,*]

[a] School of Remote Sensing and Geomatics Engineering, Nanjing University of Information Science & Technology, Nanjing, 210044, China
[b] School of Surveying and Land Information Engineering, Henan Polytechnic University, Jiaozuo, 454000, China
[c] Shanghai Astronomical Observatory, Chinese Academy of Sciences, Shanghai, 200030, China

ARTICLE INFO

ABSTRACT

The structural changes at the planetary boundary layer (PBL) top are very complex and closely related to climate and environmental changes. With the development of Global Navigation Satellite System Radio Occultation (GNSS RO), it provides a good opportunity to estimate and study PBL variations. In this paper, long-term variations and structures of planetary boundary layer height (PBLH) from 2008 to 2022 are investigated by the Wavelet Covariance Transform (WCT) method based on refractivity profiles from Constellation Observing System for Meteorology, Ionosphere, and Climate (COSMIC) and Korea Multi-purpose Satellite-5 (KOMPSAT-5). Furthermore, the temperature and pressure of PBL top are detected using the temperature and pressure profiles from COSMIC and KOMPSAT-5 occultation data. The results demonstrate the latitudinal distribution of the PBL top height, temperature, and pressure, with the more apparent temperature's latitudinal characteristics. The pressure is more strongly correlated with PBL height than temperature. The PBL height in most land and oceans is high in summer and low in winter, and the PBL pressure is low in summer and high in winter, according to seasonal variation characteristics. The global PBL temperature is high in summer and low in winter, which is more obvious in high latitude region. A positive correlation between latitude and the magnitude of seasonal variation in PBL temperature is observed worldwide. Seasonal variation is less pronounced in the Southern Hemisphere (SH) than in the Northern Hemisphere (NH) due to sea-land differences. The annual average value of the global PBL height, temperature, and pressure do not change significantly over the long term, and also there is no a discernible upward or downward trend.

1. Introduction

The Planetary Boundary Layer (PBL) is a layer between the surface and the free atmosphere, which is the lowest level of the atmosphere and is directly influenced by the surface (Patil et al., 2013). The PBL is characterized by the turbulent mixing of moisture, heat, momentum, and atmospheric tracers (such as chemical pollutants) and serves as a transition layer for the upward and downward exchange of matter, energy, and momentum in the Earth's atmosphere (Ao et al., 2012). The characteristic of the PBL itself, as well as the transfer of heat and water vapor between it and the free atmosphere and the ground, are directly related to the variety, evolution, and number of clouds that cover the PBL and have an impact on the production and dispersion of air pollution (Ramanathan et al., 1989). Above the PBL is the Free Troposphere (FT). The exchange of mass between the PBL and the FT is mainly

realized through transport processes, including friction transport and convective transport. The transfer of gases and particulate matter between the PBL and the FT is a very important process. For example, particulate matter 2.5 ($PM_{2.5}$) is the major air pollutant in many parts of the world. Once $PM_{2.5}$ enters the FT, its lifetime will be extended. Meanwhile, the scope of pollution will also be expanded (Jin et al., 2022b). The mass transfer and diffusional uptake rates of gases in liquid and solid hydrometeors are influenced by lots of factors, such as wind speed, wind direction, and the concentration of particulate matter. During storm events, strong winds in the storm speed up the movement of liquid and solid hydrometeors, and lead to transfer faster. The concentration of particulate matter affects the uptake rates of liquid and solid hydrometeors and promotes the formation and growth of hydrometeors.

One crucial factor used to describe the PBL is its height. The PBL

---

height refers to the depth of air next to the Earth's surface, which is most affected by the resistance to the transfer of momentum, heat, or moisture across the surface. The PBL height distinguishes between the boundary layer and the free atmosphere. In addition, the physical, chemical, and radiative processes of the atmosphere within the boundary layer are impacted by changes in temperature and pressure at the PBL top.

For a long time, measurements of the PBL top are mainly made by radar observations (acoustic radar, wind profile radar), radiosonde, satellite-based remote sensing observations, and model reanalysis data, but all these data have their drawbacks when applied to the PBL top sounding at large spatial scales and long time series. Radar observations have limited resolution and are susceptible to the effects of advection transport and background noise (Russell et al., 1974; Beyrich, 1997; Kumar and Jain, 2006). The limited geographical distribution of radiosonde data makes it difficult to support global-scale PBL top detection. In addition, the displacement in the horizontal direction may lead to distortion of the data (Pfenninger et al., 1999). Low vertical resolution is a problem with both reanalysis data and satellite-based remote sensing data. Nowadays, Global Navigation Satellite System (GNSS) can estimate atmospheric parameters (Jin and Su, 2020; 2021; Jin et al., 2022a), particularly GNSS Radio Occultation (Darrag et al., 2022), which can detect PBL.

The detection of PBL from the radio occultation has been proposed in 1994. Early Von Engeln et al. (2005) successfully detected the height of PBL top (PBL height) using CHAMP data, but the closed-loop mode of this data made its signal tracking capability in low tropospheric occultation poor (Gou et al., 2009). The new generation of detection missions represented by COSMIC, KOMPSAT-5, Fengyun-3C (FY–3C), and Fengyun-3D (FY-3D) significantly have increased the accuracy of occultation observations at low altitudes by implementing open-loop tracking technology on occultation receivers. The vertical resolution, spatial coverage, and temporal coverage shortcomings of conventional PBL detection methods have been successfully addressed by GNSS RO. Furthermore, it is unaffected by clouds and rain, has a large and stable data volume, and is the perfect information for identifying the PBL top (Zhran and Mousa, 2022). Basha and Ratnam (2009) used occultation bending angle profiles to identify the PBL height, which is more accurate and robust but complex. Ratnam and Basha (2010) used occultation humidity and temperature profiles to identify the PBL height, but the accuracy of this method is low. In contrast, Sokolovskiy et al. (2006) identified the PBL height using occultation refractivity profiles and verified its viability by contrasting it with reanalysis and radiosonde data. After that, Ao et al. (2012) used the gradient method to identify the PBL height from refractivity profiles and quantified the applicability of the gradient method by defining the "sharpness parameter", and Ratnam and Basha (2010) used the WCT method to identify the PBL height and successfully obtained the global PBL height distribution with high accuracy.

Most of the previous studies on the changes of global PBL top were based on short data time series (Chan and Wood, 2013; Xu et al., 2018; Basha et al., 2019; Kalmus et al., 2022), and long-term structure and variations characteristics of Global Planetary Boundary Layer Top are not clear. Moreover, previous studies mainly focused on the PBL height, while the long-term changes in temperature and pressure at the PBL top are not clear. In this paper, long-term variations and structures of planetary boundary layer height (PBLH) from 2008 to 2022 are investigated by the Wavelet Covariance Transform (WCT) method based on refractivity profiles from Constellation Observing System for Meteorology, Ionosphere, and Climate (COSMIC) and Korea Multi-purpose Satellite-5 (KOMPSAT-5). Data and methods are shown in Section 2, results and analysis are presented in Section 3, and finally, conclusions are given in Section 4.

2. Data and methods

2.1. Data

The COSMIC wetPrf data (2008–2017) and KOMPSAT-5 wetPrf data (2018–2022) are the occultation data used in this study. The service time of various occultation missions, as well as the quantity and quality of the occultation data, are used to determine the study time for various occultation data. The wetPrf data of COSMIC and KOMPSAT-5 were obtained from the COSMIC Data Analysis and Archive Center (CDAAC) at https://cdaac-www.cosmic.ucar.edu/. The COSMIC and KOMPSAT-5 wetprf data provided by CDAAC are stable with high temporal and spatial densities, which have been used to detect PBL height. (Basha et al., 2019; Kalmus et al., 2022). WetPrf includes profiles of atmospheric temperature, refractivity, and pressure with a vertical resolution of 0.1 km and an altitude of roughly 0–40 km. COSMIC was launched in April 2006. The COSMIC occultations data account for more than half of the available global occultation statistics, and the atmosphere profiles obtained from the Integrated GPS Occultation Receiver (IGOR) receiver on board has proven to have a high level of accuracy and is widely used for global weather forecasting, climate monitoring, ionospheric and geodetic measurements (Gong, 2009). COSMIC is in service until 2020, but data volumes are minimal after 2017. COSMIC-2 starts operations in 2019, taking over from COSMIC-1. COSMIC-2 is about twice the signal-to-noise ratio compared to COSMIC-1 (Schreiner et al., 2020), but most of the PBL height identified by this occultation mission is located in the middle and low latitudes (45°N-45°S), so COSMIC-2 is difficult to be used for global PBL top detection. This paper used KOMPSAT-5 to complete the global PBL top detection from 2018 to 2022. The KOMPSAT-5 satellite was launched in 2013 into a sun-synchronous orbit. Like COSMIC, the occultation mission also carries the IGOR receiver (Choi et al., 2010). Weiss et al. (2018) conducted a series of verifications on the neutral atmospheric profiles obtained by KOMPSAT-5. The results show that the neutral atmosphere profiles of KOMPSAT-5 is of good quality and its quality is comparable to that of COSMIC. Chang et al. (2022) also analyzed the KOMPSAT-5 ionospheric profiles. The KOMPSAT-5 occultation data has been available since 2015. The average distribution and seasonal distribution of PBL parameters detected by KOMPSAT-5 data and COSMIC data are not different in the discussion on the global scale, but there are differences in the monthly mean variations of different latitude regions, so this paper uses the KOMPSAT-5 data for 2018–2022.

The validation of the PBL height identified from the occultation was done by radiosonde data (Kuo et al., 2005), which was provided by the University of Wyoming at http://weather.uwyo.edu/wyoming/. This data contains profiles of temperature, specific humidity, and pressure, and is available at fixed times each day (00 UTC, 12 UTC). The radiosonde dataset has good integrity. The radiosonde directly observes the meteorological parameters, which are usually used as the background truth value in the PBL study to verify the results obtained by GNSS RO (Chan and Wood, 2013; Santosh, 2022). The radiosonde data do not provide refractivity profiles directly but need to be converted from temperature, pressure, and mixing ratio, the method of which will be described below. The distribution of radiosonde stations used in this study is shown in Fig. 1.

2.2. Determination of PBL top parameters

In this study, the PBL height is calculated using the WCT method. There are WCT method and refractivity gradient method to detect PBL height by using occultation refractivity profile. Although the WCT method will cause the lack of successful retrieval data in some high-altitude mountainous areas such as the Qinghai-Tibet Plateau, when the occultation refractivity gradient changes are not obvious, the WCT method can still detect the PBL height, while the gradient method is not applicable. In addition, the WCT method is a robust method to detect the
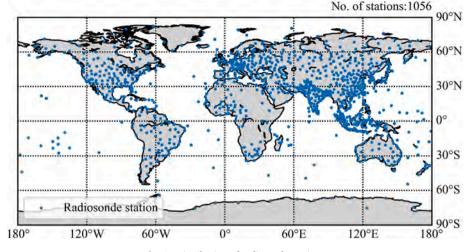
Fig. 1. Distribution of radiosonde stations.

PBL height based on the occultation refractivity data, and the PBL height has high accuracy. The essence of this method is able to detect step changes in signals. Therefore, by making appropriate changes, this method can be used to detect the height of the tropopause. The basic principle of the WCT method to detect PBL height is to perform wavelet covariance transformation on the refractivity profile to obtain the WCT profile, and PBL height corresponds to the maximum step of the profile (Liao et al., 2016). The Haar function is first defined as follows :

$$h\left(\frac{z-b}{a}\right) = \begin{cases} +1, b - \dfrac{a}{2} \le z \le b \ , \\ -1, b \le z \le b + \dfrac{a}{2} \ , \\ 0, else \ , \end{cases} \tag{1}$$

where z is the vertical height of the profile, a is the scale factor of the Haar function, b is the center position of the Haar function, the following formula can be obtained by performing wavelet covariance transformation on the Haar function:

$$W_f(a,b) = \frac{1}{a}\int_{Z_{bottom}}^{Z_{top}} f(z)h\left(\frac{z-b}{a}\right)dz \tag{2}$$

where $f(z)$ is the refractivity profile to be analyzed, Z_{top} and Z_{bottom} are the top and bottom of the refractivity profile, respectively, a is the scale factor, the larger the scale factor, the more obvious the wavelet covariance series function fluctuation, but the fluctuation information in the low-level range may be lost. Ratnam and Basha (2010) and Xu et al. (2018) have proved the optimal solution when the scale factor is $a = 0.4$ km, so this paper adopted this value as the scale factor.

The radiosonde data was used to verify the PBL height that was identified from COSMIC occultation data. The radiosonde data is the ideal background information to be used for the analysis of the retrieval results because it has high confidence and accuracy in meteorological analysis and processing. Based on the radiosonde data for the entire year of 2008, COSMIC was matched with the radiosonde data in this study using the matching principle of Kuo (Kuo et al., 2005) (time window ±1 h, spatial window ±100 km). In addition, the refractivity of the radiosonde data was obtained from the temperature, air pressure, and water vapor mixing ratio, and the equation is as follows:

$$r = \frac{e}{P-e} \tag{3}$$

$$N = 77.6\frac{P}{T} + 3.73 \times 10^5\frac{e}{T^2} \tag{4}$$

where r is mixing ratio in g/kg, T is temperature in Kelvin, P is atmospheric pressure in hPa, N is refractivity.

GNSS occultation data have the advantages of high vertical resolution and large data volume compared with radiosonde data. This paper adopted Zhu's practice (Zhu et al., 2021), based on the COSMIC data whose feasibility had been verified, to verify the retrieval results of the KOMPSAT-5 data, and its spatio-temporal matching principle is the same as above.

2.3. Analysis method

This paper divided the world into 90 × 180 grids according to the size of 2° × 2°. Each grid's PBL top parameters were determined as follows:

$$\begin{cases} \overline{P}^{a,b} = \dfrac{\sum\limits_{i=1}^{n} P_i^{a,b}}{n} \\ \lambda^{a,b} = 90° - r_\lambda \times \left(a - \dfrac{1}{2}\right) \\ \varphi^{a,b} = r_\varphi \times \left(b - \dfrac{1}{2}\right) - 180° \end{cases} \tag{5}$$

where $P_i^{a,b}$ is the parameter of the i-th PBL in the (a, b)th grid, n is the total number of parameters identified in this grid in a specific time period. r_λ and r_φ are the latitude resolution and longitude resolution of the grid, respectively. $(\lambda^{a,b}, \varphi^{a,b})$ are the coordinates of the center of the (a, b)th grid. Additionally, the global PBL top structure has the characteristics of latitudinal distribution and variation by latitude. Meanwhile, in order to explore the long-term changes of the PBL top. In this study, the globe was evenly divided into 6 latitude regions from north to south at 30° intervals, and the trends of different time series of different latitude regions were analyzed with the monthly average value as the time unit.

3. Results and analysis

3.1. Identification of the PBL height

The PBL height of refractivity profile pairs identified after spatio-temporal matching between the radiosonde data and COSMIC data for the whole year of 2008 and COSMIC and KOMPSAT-5 data for the whole year of 2018 were counted respectively. A total of 234 and 161 pairs of

profile pairs with successful PBL height retrieval were obtained, and their scatter plots are shown in Fig. 2. It can be seen from the left figure that the difference between the PBL height detected by radiosonde data and the PBL height detected by COSMIC data is mostly within 1 km, and very few exceed 1.5 km. It is completely feasible to use COSMIC to detect PBL height. The figure on the right shows the difference between COSMIC and KOMPSAT-5 profile pairs to detect PBL height results. It can be seen from the right figure that only a few profile pairs have a difference greater than 1.5 km, most of the points are still within the difference of 1 km. Fig. 2 illustrates the accuracy of COSMIC load and KOMSAT-5 in detecting PBL height.

Fig. 3 shows examples of PBL height retrieved by three sets of COSMIC and KOMPSAT-5 matched profile pairs. The blue solid lines respectively represent the function values obtained from the COSMIC and KOMPSAT-5 refractivity profiles after wavelet covariance transformation, and the red dotted line is the height of the largest step in the WCT value, namely PBL height. The three pairs of profiles in the figure are: (a) COSMIC: 2018.017.07.22.G03 and KOMPSAT-5: 2018.017.07.20.G03; (b) COSMIC: 2018.027.05.20.G22 and KOMPSAT-5: 2018.027.05.52.G03; (c) COSMIC: 2018.059.23.29.G13 and KOMPSAT-5: 2018.059.22.30.G21. In the above numbering, the first to fourth digits represent the year, the fifth to seventh digits represent the day of the year, the eighth to ninth digits represent the hour (UTC), the tenth and eleventh digits represent the minute (UTC), and the last three digits represent the GNSS satellite id. The times and locations of the three profile pairs are marked in Fig. 3. It can be seen from Fig. 3 that the WCT value sequences retrieved by the IGOR loads carried by COSMIC and KOMPSAT-5 respectively show strong volatility, and the abruptness of the two is also very obvious, indicating that the refractivity profiles contain rich details. Combining the information in Figs. 2 and 3, the PBL height can be successfully detected using COSMIC and KOPMSAT-5.

Fig. 4 shows the distribution of occultation observation files that successfully retrieve the PBL height from 2008 to 2022 (resolution 2° × 2°). As shown in the figure, the occultation observation files with successful retrieval show obvious latitudinal and sea-land differences. The distribution of occultation observation files is higher in the 15°N-60°N and 15°S-60°S regions than in the equatorial and polar regions. The influence of the observation angle between the occultation satellites and GNSS satellites makes the highest distribution of qualified retrieval occultation observation files occur near 45°N and 45°S, with about 150–200 qualified retrieval occultation observation files per grid in this time period. In tropical region and high-altitude polar region, the number of qualified retrieval occultation observation files is relatively low, and the tropical region is mainly affected by high moisture levels and spatial variations of moisture (Ao et al., 2012). In addition, the

topography of highlands or mountains such as the Himalayas and the Andes also causes the lack of occultation refractivity information or poor quality of the profile (Zhu et al., 2021), thus leading to the lack of qualified retrieval occultation observation files. The number of successfully retrieved occultations at the same latitude in the ocean is larger than that in the land, which is the reason why the number of successfully retrieved occultations in the SH is larger than that in the NH.

Table 1 shows the 2008–2022 COSMIC and KOMPSAT-5 data, the 2008–2017 COSMIC data, and the 2017–2022 KOMPSAT-5 data in different seasons of qualified retrieval files and the mean and standard deviation of the three PBL parameters. The PBL height and PBL temperature detected by KOMPSAT-5 data are slightly larger than those obtained by COSMIC, and the PBL pressure detected by KOMPSAT-5 data is slightly smaller than that obtained by COSMIC. The standard deviation of the detection results of KOMPSAT-5 data is slightly larger than that of COSMIC. In general, the mean, as well as standard deviation results obtained from KOMPSAT-5 and COSMIC statistics, are similar. Since the number of COSMIC's qualified retrieval files is greater than the number of KOMPSAT-5's qualified retrieval files in this study, the overall statistics were skewed in favor of the COSMIC detections. It can be seen from the table that COSMIC and KOMPSAT-5 data have the largest number of observations in the MAM (March-April-May) season and the least number of observations in the SON (September-October-November) season. For PBL height and PBL temperature, the maximum values of COSMIC and KOMPSAT-5 data both appear in JJA (June-July-August), and the minimum values appear in DJF (December-January-February). PBL temperature is more variable across the seasons compared to PBL height. The maximum value of PBL pressure for COSMIC and KOMPSAT-5 data occurs at DJF and the minimum value at JJA, which is consistent with the basic relationship between pressure and altitude. In terms of the dispersion of the data for the three parameters, PBL temperature has the largest standard deviation, indicating that there is a large variation in the values of PBL temperature across the globe.

3.2. Global distribution and variations of PBL height

Fig. 5 shows the distribution of the average height of the PBL top from 2008 to 2022. On the terrestrial side, the regions with higher PBL height (>2.5 km) mainly occur from north to south mainly in the Iberian Peninsula, the Arabian Peninsula, the Sahara Desert in northern Africa and west-central Africa, central Indian Peninsula, south-central South America, southern Africa, and the northwestern region north of 30°S in Australia. In these regions, the high temperature and low rainfall throughout the year and the low atmospheric water content lead to the high position of atmospheric turbulence, and from the perspective of
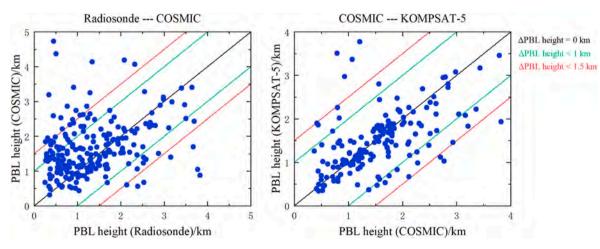

Fig. 2. Scatter plot of PBL height retrieved from refractivity profile pairs.
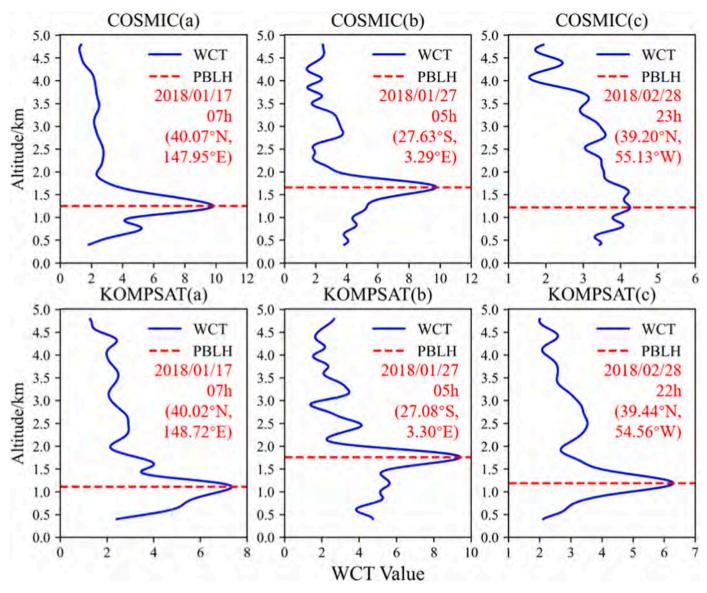
Fig. 3. Comparison of PBL height retrieval from WCT profiles of KOMPSAT-5 and COSMIC.

turbulent motion, the density of the lowest air layer where turbulence persists is the PBL height (Dai et al., 2014), so the PBL height is high in these regions. In terms of sea area, the highest value of PBL height (2.0–2.5 km) occurs in the middle and low latitude region (45°N-45°S). Within this region, the PBL height is relatively low in the coastal waters of the North and South American, North and South African continents, and there are two possible reasons for this phenomenon. The first reason is that this phenomenon may be due to strong subsidence and relatively cold upwelling water (Guo et al., 2011). Another reason is that the PBL height on the ocean is closely related to the cold or warm ocean current, and the above-mentioned lower PBL height area overlaps with the cold ocean current area. These areas are accompanied by downdrafts and the height of inversion layer is relatively low. In addition, the PBL height is relatively low from the Bay of Bengal to the South China Sea to the Banda Sea and other waters off Indonesia. The PBL height is generally higher in the region except for the above-mentioned areas. The highest values (>2 km) are reached in the eastern part of Madagascar, the south-central part of the eastern Pacific Ocean, and part of the southern Atlantic Ocean. In contrast, the PBL height is generally low in the middle and high latitude seas, and the closer to the poles, the smaller the PBL height value is. Within this latitude region, the PBL height in the same latitude sea is approximately the same, indicating that the PBL height in

this region is mainly determined by latitude. In terms of sea-land differences, because the annual average temperature of the ocean at the same latitude is lower than that of the land, the water content of the atmosphere is high, and the air pressure over the ocean is relatively high, resulting in relatively weak atmospheric turbulence (Xu et al., 2018). In addition, the boundary layer on the ocean is less exposed to solar radiation than the land. Therefore, the PBL height of the ocean is lower than that of the land at the same latitude.

Fig. 6 shows the variation of PBL height in different seasons. At low latitude land (30°N-30°S), seasonal variations are significant in northern Africa, the Arabian Peninsula, and northwestern Australia, where PBL height is locally high in summer and low in winter. These regions are dry and have little rain, and PBL height shows a strong agreement with solar insolation and land surface temperature. Its seasonal variations coincide with trends in the absorption and radiation of heat by the land surface. As the surface heats the atmosphere, the upward lift of air masses triggers the development of the turbulent boundary layer, raising the boundary layer height. The opposite phenomenon is found in east-central South America, where PBL height is lower than JJF during DJF, a phenomenon contrary to the observation of Xu et al. (2018), and the same as that of Basha et al. (2019). At low latitude sea, the PBL height is lower in summer and higher in winter in the central Pacific
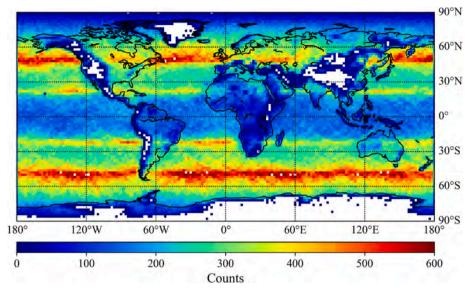
Fig. 4. Distribution of qualified retrieval occultation observation files.

Table 1
Statistics of qualified retrieval files and PBL parameters in different seasons.

Season	Qualified retrieval files	PBL height (km)	PBL temperature (°C)	PBL pressure (mbar)
Total				
MAM	870034	1.56 ± 0.78	2.13 ± 13.65	838.51 ± 87.56
JJA	852139	1.58 ± 0.79	4.43 ± 13.18	838.15 ± 89.08
SON	797714	1.54 ± 0.77	2.27 ± 13.74	839.96 ± 86.52
DJF	823999	1.53 ± 0.77	1.46 ± 14.51	840.67 ± 89.83
COSMIC				
MAM	777033	1.56 ± 0.78	2.02 ± 13.41	838.61 ± 86.01
JJA	768763	1.57 ± 0.78	4.36 ± 12.97	838.40 ± 87.44
SON	716603	1.54 ± 0.76	2.12 ± 13.58	840.05 ± 85.50
DJF	735960	1.53 ± 0.78	1.37 ± 14.22	840.57 ± 86.91
KOMPSAT-5				
MAM	93001	1.58 ± 0.84	3.06 ± 15.43	837.70 ± 99.63
JJA	83376	1.61 ± 0.85	5.15 ± 14.97	835.83 ± 102.89
SON	81111	1.56 ± 0.83	3.54 ± 15.06	839.13 ± 95.00
DJF	88039	1.54 ± 0.83	2.16 ± 16.73	841.50 ± 111.27

Ocean in the NH and the mid-Atlantic Ocean in the NH. On the contrary, the PBL height in the central Pacific Ocean in the SH, the central Atlantic Ocean in the SH, and most of the Indian Ocean are high in summer and low in winter. The above phenomenon indicates that the value of PBL height in the low latitude ocean is not overly influenced by heat. This region is under the control of the north-south subtropical high pressure, and high temperature throughout the year, so the seasonal variation of the sea temperature is not obvious. The solar radiation received by the sea is mainly used for the evaporation process of seawater, which has a weak influence on the air temperature, on the other hand, the excessive cloud cover also reduces the solar radiation received by the sea surface (Basha and Ratnam, 2009). These two regions are in the northeast trade wind belt and southeast trade wind belt in summer and in the sub-tropical high pressure belt in winter (Xu et al., 2018), resulting in the

phenomenon that the PBL height of the former is low in summer and high in winter, and the PBL height of the latter is high in summer and low in winter. In the North Atlantic Ocean near the equator and in the West Pacific Ocean off the east coast of Asia, the phenomenon of low PBL height in summer and high PBL height in winter is also observed. The low summer PBL height in the North Atlantic near the equator is influenced by the temperature difference between the sea and air or fog in summer (Von Engeln and Teixeira, 2013; Seidel et al., 2012), while the low summer PBL height in the East Coast of Asia is influenced by the frequent occurrence of typhoons in this region in summer and autumn. Similarly, the Gulf of Mexico region also has lower PBL height in summer due to the frequent occurrence of typhoons in the region during the season. However, the Gulf of Mexico region is affected by the movement of the polar cold snap toward the equator and the offshore fronts in winter, so the PBL height in the Gulf of Mexico region is higher in winter. The movement of polar cold air masses toward the equator, cold air outbreaks, and offshore frontal systems are a few of the factors that affect the high PBL height in winter in the North Atlantic near the equator (Liao et al., 2015), whereas the high PBL height in the West Pacific East Coast of Asia is influenced by winter cold waves or strato-cumulus clouds generated by the Hardly circulation (Klein and Hart-mann, 1993). The eastern South Pacific, the eastern waters of South America, the southern Indian Ocean waters in eastern Australia, and the eastern Pacific Ocean waters north of the United States are located in the trade wind area all year round and are less affected by seasonal changes, so they correspond to higher PBL height. In the mid-high latitude land, the PBL height transitions from the highest value in summer to the lowest value in winter. The increase in land surface temperature and the decrease in static stability are the reasons why the PBL height in this region reaches the highest value in summer (Chan and Wood, 2013). The value of the PBL height in this region is positively correlated with the heat absorbed by the ground and radiated by the sun. Seidel et al. (2012) also demonstrated in their research that the increase of land surface temperature is the main determinant of the maximum PBL height in Europe in summer. In addition, the magnitude of seasonal variation differs for land areas above 30° in the NH and SH, with stronger seasonal variation in the NH because of its larger land area and more continental nature. The seasonal variation of PBL height, which is higher in summer and lower in winter, also appears in the sea area of 30°N-50°N and 30°S-50°S, but the seasonal variation in this area is relatively weak. Warm advection from the shallow wet layer in the tropics results in relatively high PBL height. In high latitude oceans, the seasonal varia-tion is further strengthened, and the sea area north of 60°N is about
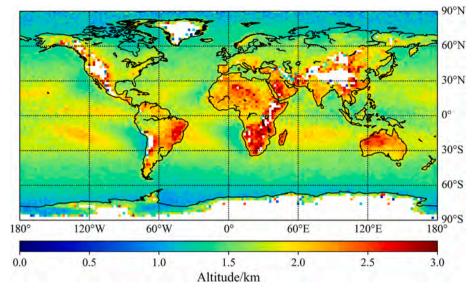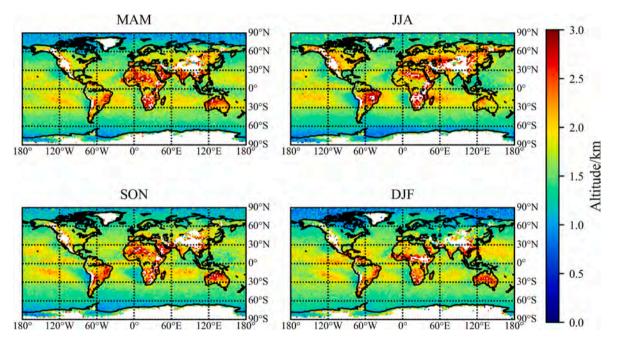
Fig. 5. 2008–2022 global PBL height.

Fig. 6. Global seasonal variation of PBL height, MAM refers to March-April-May, JJA refers to June-July-August, SON refers to September-October-November, DJF refers to December-January-February.

0.5–1 km higher in summer than in winter, which is due to the change of sea ice density. In summer, the density of sea ice decreases, and the rise in sea temperature generates turbulent kinetic energy, which is conducive to deepening the PBL. The lower PBL height in winter near Antarctica is due to the fact that ice extending to this latitude in winter provides a cold surface for the atmosphere, minimizing any instability (Zhu et al., 2021), resulting in lower PBL height. Analyzed from the perspective of sea-land differences, the PBL height seasonal climatology of land areas is more obvious than that of the ocean due to the large diurnal temperature difference at the surface, which is also consistent with the results obtained by Xu et al. (2018).

The 15-year PBL height variation of the different latitude regions from 2008 to 2022 in terms of months is shown in Fig. 7. The black line in the figure distinguishes the detection time of different satellites. The PBL height after 2018 is obtained from KOMPSAT-5, and it is COSMIC before 2018. Fig. 7 shows a small difference between KOMPSAT-5 and

COSMIC in the detection of PBL height, which is mainly reflected in the fact that the peaks of KOMPSAT-5 detection results in low latitudes (30°N-30°S) in 2018 and 2019 are higher than those of COSMIC. In addition, the peak value in 2018 in the 30°N-60°N region is also slightly higher, while the valley value in 2020 and 2022 in the 60°N-90°N region is correspondingly lower. The PBL height at low latitudes is higher than the PBL height at high latitudes due to the fact that low latitudes are exposed to larger values of solar radiation and surface radiation compared to high latitudes, thus elevating the boundary layer. The seasonal climatology of PBL height exists in different latitude regions of the globe, and the seasonal variation of PBL height is larger in high latitude than in low latitude and larger in the NH than in the SH. Due to the higher heat capacity of the ocean and the reflection of the solar short-wave radiation by the clouds above the ocean, the seasonal variation of the PBL height of the ocean is smaller than that of the land. The proportion of ocean in the SH and high latitude region is larger than that
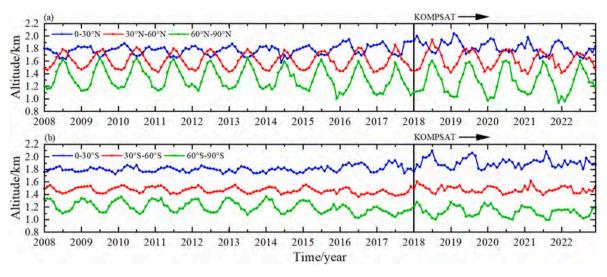
Fig. 7. Variation of PBL height in different latitudes from 2008 to 2022. (a) Trends in the NH, (b) Trends in the SH.

in the NH and high latitude region, leading to the above phenomenon. Additionally, because seasonal changes in PBL height are more pronounced in the NH than in the SH, the trend in the NH is more wave-like. And more areas in low latitude region are hot, dry, and less rainy throughout the year is thought to be the reason why the seasonal variation of PBL height in low latitude region is not as obvious as those in high latitude region. The most significant PBL height seasonal variation is found in the area above 60°N, and the variation of sea ice density has a large impact on the PBL height in this area. In addition, the detection results are lower in the 60°S-90°S region in 2016, 2017, 2021, and 2022, and the above results may be influenced by the fact that COSMIC and KOMPSAT-5 are each in the later stages of service during the time period. Ignoring the effects of different detection occultation loads, the PBL height in different latitude regions of the globe has a regular seasonal variation and the values remain stable from 2008 to 2022.

3.3. 2008–2022 global distribution and variations of PBL temperature and PBL pressure

Figs. 8 and 9 show the average temperature and pressure at the top of the boundary layer from 2008 to 2022, respectively. Both temperature

and pressure have the characteristics of distribution by latitude. Global PBL temperature is mainly determined by latitude and has little relationship with longitude and other factors, while PBL pressure is mainly determined by altitude. In addition, there is a clear feature of equatorial symmetry in the PBL temperature. Compared with Fig. 5, both of them have a correlation with PBL height. The correlation of temperature is shown as a negative correlation with altitude in low latitudes (30°N-30°S), and a positive correlation in 40°N-90°N and 40°S-90°S latitudes. Pressure is negatively correlated with altitude globally. Pressure is more influenced by PBL height than temperature. The highest value of temperature occurs in the region of 30°N-30°S. The maximum value of temperature in the area can be above 20 °C. Additionally, the PBL temperature in the oceanic region at the same latitude is higher than that of the land. Temperature is mainly influenced by latitude, properties of the subsurface, and altitude (Xu et al., 2018), and in this region, PBL temperature is mainly influenced by altitude. The 30°N-40°N and 30°S-40°S are the transition zones of PBL temperature, and the PBL temperature in this area is kept at about 10 °C. The PBL temperature in the NH and SH above this latitude begins to decrease gradually according to latitude. In the region of 40°N-90°N and 40°S-90°S, PBL temperature decreases with increasing latitude, and the lowest value
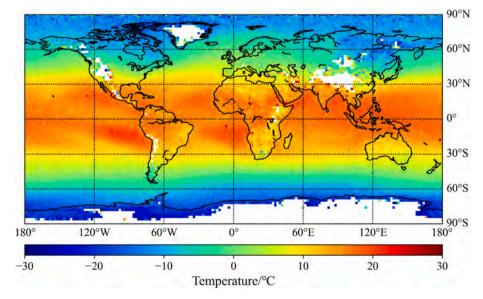

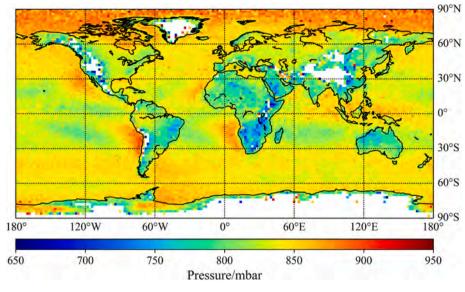**Fig. 8.** 2008–2022 global PBL temperature.

Fig. 9. 2008–2022 global PBL pressure.

occurs in the region south of 60°S. The minimum can be less than −20 °C. The PBL temperature near the South Pole is lower than that of the North Pole. The PBL temperature is lower along the east coast of North America and the east coast of Eurasia than the land and ocean at the same latitude. In terms of pressure, the pressure in the land area at the same latitude is significantly lower than that in the ocean, which is consistent with the distribution characteristics of PBL height, which is higher than that in the ocean at the same latitude, and the height is negatively correlated with pressure. In addition, the average PBL temperature of the land area is higher than that of the ocean, which leads to a lower atmospheric density compared with the ocean and contributes to the formation of this phenomenon. The PBL pressure shows significantly high values (>850 mbar) in the waters off the west coast of the North and South American continents, the waters off the west coast of Africa, and the waters above 60°N. The lowest values (<800 mbar) are found in the eastern Pacific Ocean, the mid-Atlantic Ocean, and the eastern

Madagascar Sea. The highest values on land are found in the regions far from the coastline in Eurasia and North America, and the lowest values are found in northwestern and southern Africa, central-eastern South America, the Arabian Peninsula, the east coast of Asia, and northwestern Australia. The difference between the maximum values is about 100 mbar. Compared with Fig. 5, there are similar distribution characteristics in Fig. 9, but the values are opposite. In the 2008–2022 global average pressure distribution, PBL height is the decisive factor in determining PBL pressure.

The seasonal variation of the global PBL temperature from 2008 to 2022 is shown in Fig. 10. According to the figure, the PBL temperature has similar distribution characteristics with Fig. 8 in all seasons, showing a clear latitudinal distribution with equatorial symmetry and a negative correlation between the PBL temperature and latitude. There was no significant relationship between PBL temperature and longitude in all seasons. In addition, the seasonal variation of the PBL temperature
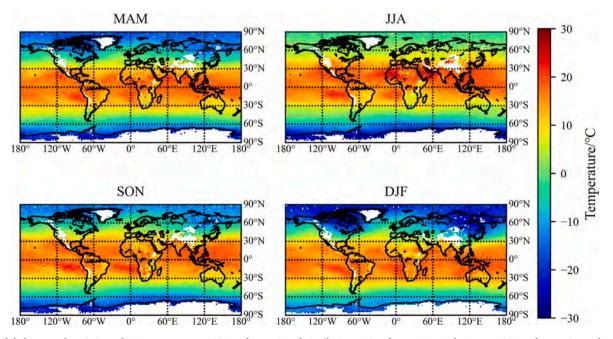

Fig. 10. Global seasonal variation of PBL temperature, MAM refers to March-April-May, JJA refers to June-July-August, SON refers to September-October-November, DJF refers to December-January-February.

is also significant, with the temperature reaching its highest value in the local summer and lowest value in the winter. The transition period is spring and autumn, and PBL temperature has similar distribution characteristics in these two seasons, but the value is lower in spring than in autumn in the region of 60°N-90°N. The 45°N-90°N and 45°S-90°S region has more pronounced seasonal variations than the 45°N-45°S region due to its greater alteration of thermal radiation over the course of the year than the 45°N-45°S region. In the middle and high latitude region of the NH, the PBL temperature increases continuously from spring to summer, and reaches the maximum value in a year in summer, and the maximum value can reach 10 °C. The seasonal variation of PBL temperature in the middle and high latitude region of the NH is greater than that in the middle and high latitude region of the SH. The difference in the properties of the underlying surface caused this phenomenon. The ocean area in the SH is larger, and the heat capacity of the ocean is larger, which leads to the insignificant temperature rise of the PBL temperature in the middle and high latitude regions of the SH. Seasonal variation characteristics of temperature exist in low latitude region, but their value is relatively high in all seasons. The PBL temperature in low latitude region is above 15 °C in all seasons. The PBL temperature in the eastern part of Eurasia and eastern part of North America is lower than the land at the same latitude in all seasons. The temperature transition zone of about 10° in the NH and SH (about 10 °C) mentioned above occurs in all seasons, and it gradually moves southward from the JJA to DJF period. The above phenomenon is more likely to be caused by the variation of solar radiation energy. In addition, this study also finds that the areas with lower PBL temperature (<-10 °C) in the NH during the winter period are much higher than the areas with this value in the SH. The regions above 60°N in the NH have PBL temperatures below −10 °C during DJF, while the SH reaches this value only near the poles. From the perspective of sea-land differences, the PBL temperature in the ocean area is higher than that of the land at the same latitude. There is no significant difference in the magnitude of seasonal variation of PBL between marine and land regions.

Fig. 11 shows the monthly mean variation of the PBL temperature in different latitude regions from January 2008 to December 2022. The seasonal variation and magnitude of different latitude regions are the same as the information expressed in Fig. 11. It is also evident from Fig. 10 that latitude is negatively correlated with the magnitude of PBL temperature and positively correlated with the magnitude of PBL temperature change. But from Fig. 11, we can find that the magnitude of boundary layer top temperature variation in the SH is not as significant as that in the NH, and this information is difficult to obtain in Fig. 10. Differences in sea and land areas contribute to the phenomenon. The sea area of the SH is larger than that of the NH, and seawater, as a subsurface, has a higher heat capacity, resulting in less significant changes in PBL temperature in the SH than in the NH. PBL temperature is mainly influenced by PBL height, latitude, and underlying surface properties. So

the seasonal variations are more pronounced at high latitudes than at low latitudes in Fig. 11. In terms of the underlying surface properties, the temperature change is more significant in the land area than in the sea area, in addition, the seasonal change of PBL height is more significant in the land area than in the sea area, and the proportion of the ocean in the NH is lower, so the seasonal change of the PBL temperature in the NH is more significant and more wave-like. The temperature trends in the NH and SH differ by half a cycle, with their temperature change curves all peaking in the local summer and reaching a trough in the winter. It shows that the PBL temperature is mainly affected by solar thermal radiation. Affected by the service time of KOMPSAT-5, the detection of seasonal variation characteristics in the 0–30°S region after 2020 is not obvious. The variation of the monthly average of the global PBL temperature in different latitudes from 2008 to 2022 is stable and regular, and the values of different months in each year are similar, and the global PBL temperature has not changed significantly in that decade.

The seasonal variation characteristics of the global PBL pressure from 2008 to 2022 are given in Fig. 12. As with temperature, the distribution characteristics of barometric pressure in different seasons are similar to Fig. 9, but the values are different in different seasons. The most significant region of seasonal variation is the 60°N-90°N region. In Eurasia, northern North America, northern Africa, eastern South America, the area north of 30°S in Australia, and some sea areas from 60°S to 90°S, the PBL pressure is low in summer and high in winter. The opposite phenomenon is found in the waters off the west coast of the East Pacific continent in the NH, the waters off the west coast of Africa in the NH, the South China Sea and the waters east of the South China Sea, and the waters off Indonesia, where the pressure is high in summer and low in winter. The waters off west of South America in the SH and the waters off west Africa in the SH their highest values during the JJA-SON period. Compared with Fig. 6, it is found that the air pressure distribution in the above-mentioned areas is just opposite to the PBL height. The values of pressure are related to thermal, altitude, and atmospheric dynamics, among which altitude is the dominant factor, leading to the seasonal characteristics of pressure mentioned above. It can also be concluded from Fig. 12 that the PBL pressure in the land area is lower than the PBL pressure in the sea area in all seasons. There are three main reasons for the phenomenon. Firstly, in the same latitudinal band, the average temperature is higher in the land area than in the sea, resulting in lower atmospheric density in the land area. Secondly, the pressure is negatively correlated with altitude, while PBL height is higher in the land area than in the sea area. Finally, the land area is more controlled by the subtropical high pressure than the sea area, leading to the above phenomenon (Xu et al., 2018). Fig. 12 illustrates that PBL pressure is not only negatively correlated with PBL height in the global average distribution, but its distribution characteristics in each season are also mainly determined by PBL height.

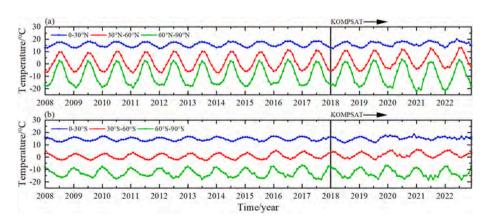The variation of the monthly mean of PBL pressure from 2008 to

Fig. 11. Variation of PBL temperature in different latitudes from 2008 to 2022. (a) Trends in the NH, (b) Trends in the SH.
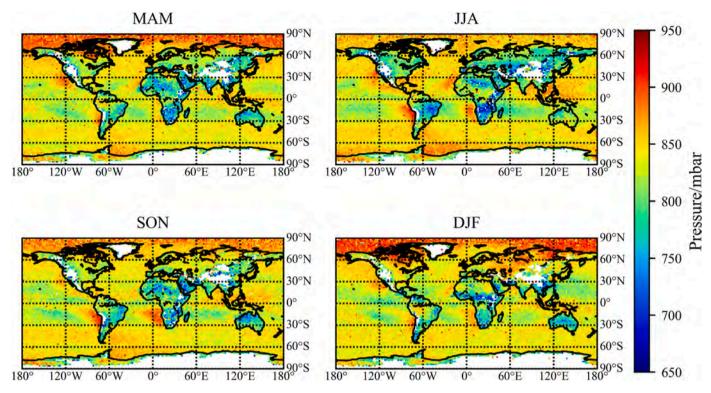
Fig. 12. Global seasonal variation of PBL pressure, MAM refers to March-April-May, JJA refers to June-July-August, SON refers to September-October-November, DJF refers to December-January-February.

2022 in different latitude regions is given in Fig. 13. The differences between KOMPSAT-5 and COSMIC for PBL pressure are mainly reflected in the insignificant seasonal variation of KOMPSAT-5 for the 0°-30°S region, and the detected troughs are significantly lower than those obtained by COSMIC. In addition, KOMPSAT-5 detects anomalously high PBL pressure for the 60°N-90°N region in February 2021. The highest values of PBL pressure occur at 60°N-90°N and the lowest values occur at low latitude region. Since PBL pressure is mainly affected by PBL height, the seasonal variation of PBL height in high latitude region is larger than that in low latitudes, resulting in a similar phenomenon in the seasonal variation of PBL pressure. The NH has more land mass and is more continental, its seasonal variation is more pronounced than that of the SH. Compared with Figs. 7 and 11, Fig. 13 has a different period curve, with both peaks and troughs half a period away from the image of the change in elevation and temperature, which is consistent with the relationship between pressure, temperature, and elevation. In the above, it has been discussed that PBL pressure has a strong negative correlation with PBL height both in the average distribution and seasonal climate

characteristics from 2008 to 2022. Compared with Fig. 7, the seasonal curve pattern of height is better than that of pressure, especially at low latitude region, where the seasonal variation of height is more regular than that of pressure. Considering that during this time period, the PBL pressure and PBL temperature of the 0°-30°S latitude zone were stable, and the other five curves also maintained stable characteristics during this time period. Ignoring the effects of different occultation missions, the PBL pressure remains stable over the time period.

4. Conclusions

Using the multi-source GNSS radio occultation data based WCT method, this paper investigates the distributions and trends of the global PBL height, PBL temperature, and PBL pressure from 2008 to 2022. The results show that, in terms of distribution characteristics, the PBL top height, temperature, and pressure all have a distribution pattern by latitude, among which the latitudinal distribution pattern of temperature is more obvious. In terms of the correlation of the three parameters,
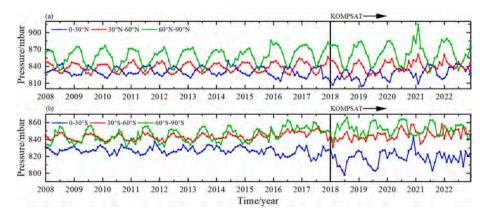

Fig. 13. Variation of PBL pressure in different latitudes from 2008 to 2022. (a) Trends in the NH, (b) Trends in the SH.

the PBL height is negatively correlated with the PBL temperature at low latitude region (30°N-30°S), while the rest of the regions show a positive correlation. For PBL pressure, whether it is the average distribution of PBL pressure in 2008–2022 or the seasonal distribution of PBL pressure, its distribution is mainly affected by PBL height, PBL pressure is negatively correlated with PBL height globally, and PBL temperature is more affected by latitude. Compared with PBL temperature, PBL pressure has a stronger correlation with PBL height. All three show sea-land differences, with the PBL height higher on land than on sea at the same latitude, while the PBL temperature and PBL pressure are lower than their marine counterparts. For seasonal variation characteristics, in most land and sea areas, the PBL height is high in summer and low in winter, and the PBL pressure is low in summer and high in winter. The temperature exhibits high values in summer and low values in winter on a global scale, and the phenomenon is more pronounced at middle and high latitude regions. The seasonal variation is more significant in the high latitude region than in the low latitude region for all three, and the seasonal variation is less pronounced in the SH than in the NH due to the sea-land differences. For the long-term variation characteristics, the PBL height, PBL temperature, and PBL pressure remain stable from 2008 to 2022.

The long-term stability of PBL top parameters has profound implications such as climate and air pollution. Many processes such as convective activity, turbulent mixing, low-level cloud formation, pollutant dispersion, and surface energy balance are present within the boundary layer. The PBL height determines the vertical extent of turbulent mixing, convective transport, and pollutant dispersion within the boundary layer, strongly influencing the development and evolution of convective activity. Variations in PBL temperature and PBL pressure affect the physical, chemical and radiative processes of the atmosphere within the boundary layer. Maintaining a stable atmospheric boundary layer means that the dispersion of pollutants does not deepen on long-term scales. In addition, the long-term stability of the PBL height is instructive for the selection of boundary layer parameterization schemes in numerical models and the inversion of aerosols. Long-term stable PBL top parameters provide potential avenues for future research. For instance, it is worthwhile to explore the global long-term trends of parameters such as $PM_{2.5}$ and precipitable water vapor (PWV), which characterize pollutant concentrations and climate change. In addition, the scale of correlation between these parameters and the PBL parameters and the spatial and temporal variations in the scale of correlation are worthy of further discussion.

In this study, the number of observations to retrieve PBL parameters in tropical and polar regions is relatively small, which should be further improved for GNSS RO detection of PBL. In addition, the fusion of different occultation data and their detections deserves further study in the future. Along with the improvement of open-loop tracking data quality and data processing capability of the new generation of occultation receivers, and the application of algorithms such as machine learning to improve the profile to enhance the accuracy of detecting PBL height, the monitoring capability of GNSS occultation for PBL structure will be further improved and studied.

Author contribution statement

Conceptualization: H.X. and S.J.; methodology: H.X. and S.J.; writing-original draft preparation: H.X.; writing-review and editing: S. J..

Declaration of competing interest

The authors declare that they have no known competing financial interests or personal relationships that could have appeared to influence the work reported in this paper.

References

Ao, C.O., Waliser, D.E., Chan, S.K., Li, J.L., Tian, B., Xie, F., Mannucci, A., 2012. Planetary boundary layer heights from GPS radio occultation refractivity and humidity profiles. J. Geophys. Res. Atmos. 117 (D16).

Basha, G., Kishore, P., Ratnam, M.V., Ravindra Babu, S., Velicogna, I., Jiang, J.H., Ao, C. O., 2019. Global climatology of planetary boundary layer top obtained from multi-satellite GPS RO observations. Clim. Dynam. 52, 2385–2398.

Basha, G., Ratnam, M.V., 2009. Identification of atmospheric boundary layer height over a tropical station using high-resolution radiosonde refractivity profiles: comparison with GPS radio occultation measurements. J. Geophys. Res. Atmos. 114 (D16).

Beyrich, F., 1997. Mixing height estimation from sodar data—a critical discussion. Atmos. Environ. 31 (23), 3941–3953.

Chan, K.M., Wood, R., 2013. The seasonal cycle of planetary boundary layer depth determined using COSMIC radio occultation data. J. Geophys. Res. Atmos. 118 (22), 12,422-12,434.

Chang, H., Chang, J., Sun, K.A., Lee, W.K., Lee, J., 2022. Preliminary results of electron density profiles retrieved from KOMPSAT-5 Radio Occultation Data. In: Proceedings of AGU Fall Meeting 2022, America, pp. P42G–P2486.

Choi, M.S., Lee, W.K., Cho, S.K., Park, J.U., 2010. Operation of the radio occultation mission in KOMPSAT-5. J. Astron. Space Sci. 27 (4), 345–352.

Dai, C., Wang, Q., Kalogiros, J., Lenschow, D., Gao, Z., Zhou, M., 2014. Determining boundary-layer height from aircraft measurements. Boundary-Layer Meteorol. 152, 277–302.

Darrag, M., Jin, S.G., Calabia, A., Samy, A., 2022. Determination of tropical belt widening using multiple GNSS Radio Occultation measurements. Ann. Geophys. 40 (3), 359–377.

Gong, X.Y., 2009. Research on GNSS atmospheric radio occultation technique. In: Doctoral Dissertation, Graduate University of Chinese Academy of Science, Beijing.

Gou, X.P., Fu, Y., Guo, Y.N., Du, X.Y., 2009. COSMIC mission and error analysis of GPS radio occultation data. J. Meteor. Sci. 29 (3), 348–354.

Guo, P., Kuo, Y.-H., Sokolovskiy, S., Lenschow, D., 2011. Estimating atmospheric boundary layer depth using COSMIC radio occultation data. J. Atmos. Sci. 68 (8), 1703–1713.

Jin, S.G., Gao, C., Yuan, L., Guo, P., Calabia, A., Ruan, H., Luo, P., 2021. Long-term variations of plasmaspheric total electron content from topside GPS observations on LEO satellites. Rem. Sens. 13 (4), 545.

Jin, S.G., Su, K., 2020. PPP models and performances from single- to quad-frequency BDS observations. Satell. Navig. 1 (1), 16.

Jin, S.G., Wang, Q., Dardanelli, G., 2022a. A review on multi-GNSS for Earth observation and emerging applications. Rem. Sens. 14 (16), 3930.

Jin, X., Cai, X., Huang, Q., Wang, X., Song, Y., Kang, L., Zhang, H., 2022b. $PM_{2.5}$ exchange between atmospheric boundary layer and free Troposphere in North China plain and its long-range transport effects. J. Geophys. Res. Atmos. 127 (22), e2022JD037410.

Kalmus, P., Ao, C.O., Wang, K.-N., Manzi, M.P., Teixeira, J., 2022. A high-resolution planetary boundary layer height seasonal climatology from GNSS radio occultations. Remote Sens. Environ. 276, 113037.

Klein, S.A., Hartmann, D.L., 1993. The seasonal cycle of low stratiform clouds. J. Clim. 6 (8), 1587–1606.

Kumar, K.K., Jain, A., 2006. L band wind profiler observations of convective boundary layer over Gadanki, India (13.5° N, 79.2° E). Radio Sci. 41 (2), 1–12.

Kuo, Y.H., Schreiner, W., Wang, J., Rossiter, D., Zhang, Y., 2005. Comparison of GPS radio occultation soundings with radiosondes. Geophys. Res. Lett. 32 (5).

Liao, Q.X., Zhao, X.F., Shi, H.Q., Huang, S.X., Xiang, J., 2015. Spatial and temporal characteristics of the boundary layer height based on COSMIC radio occultation data. J. Meteor. Sci. 35 (6), 737–743.

Liao, M., Zhang, P., Yang, G.L., Bi, Y.M., Liu, Y., Bai, W.H., Meng, X.G., Du, Q.F., Sun, Y. Q., 2016. Preliminary validation of the refractivity from the new radio occultation sounder GNOS/FY-3C. Atmos. Meas. Tech. 9 (2), 781–792.

Patil, M., Patil, S., Waghmare, R., Dharmaraj, T., 2013. Planetary Boundary Layer height over the Indian subcontinent during extreme monsoon years. J. Atmos. Sol. Terr. Phys. 92, 94–99.

Pfenninger, M., Liu, A.Z., Papen, G.C., Gardner, C.S., 1999. Gravity wave characteristics in the lower atmosphere at South Pole. J. Geophys. Res. Atmos. 104 (D6), 5963–5984.

Ramanathan, V., Cess, R., Harrison, E., Minnis, P., Barkstrom, B., Ahmad, E., Hartmann, D., 1989. Cloud-radiative forcing and climate: results from the Earth radiation budget experiment. Science 243, 57–63.

Ratnam, M., Basha, S., 2010. A robust method to determine global distribution of atmospheric boundary layer top from COSMIC GPS RO measurements. Atmos. Sci. Lett. 11 (3), 216–222.

Russell, P.B., Uthe, E.E., Ludwig, F.L., Shaw, N.A., 1974. A comparison of atmospheric structure as observed with monostatic acoustic sounder and lidar techniques. J. Geophys. Res. 79 (36), 5555–5566.

Santosh, M., 2022. Estimation of daytime planetary boundary layer height (PBLH) over the tropics and subtropics using COSMIC-2/FORMOSAT-7 GNSS–RO measurements. Atmos. Res. 279, 106361.

Schreiner, W.S., Weiss, J., Anthes, R.A., Braun, J., Chu, V., Fong, J., Hunt, D., Kuo, Y.H., Meehan, T., Serafino, W., 2020. COSMIC-2 radio occultation constellation: first results. Geophys. Res. Lett. 47 (4), e2019GL086841.

Seidel, D.J., Zhang, Y., Beljaars, A., Golaz, J.C., Jacobson, A.R., Medeiros, B., 2012. Climatology of the planetary boundary layer over the continental United States and Europe. J. Geophys. Res. Atmos. 117 (D17).

Sokolovskiy, S., Kuo, Y.H., Rocken, C., Schreiner, W., Hunt, D., Anthes, R., 2006. Monitoring the atmospheric boundary layer by GPS radio occultation signals recorded in the open-loop mode. Geophys. Res. Lett. 33 (12).

Von Engeln, A., Teixeira, J., 2013. A planetary boundary layer height climatology derived from ECMWF reanalysis data. J. Clim. 26 (17), 6575–6590.

Von Engeln, A., Teixeira, J., Wickert, J., Buehler, S., 2005. Using CHAMP radio occultation data to determine the top altitude of the planetary boundary layer. Geophys. Res. Lett. 32 (6).

Weiss, J., Auligné, T., Dutta, S., Huelsing, H., Jung, O., Kuo, B., Lee, W., Schreiner, W., Sleziak-Sallee, M., VanHove, T., Yoon, Y., Zhang, H., 2018. KOMPSAT-5 GNSS radio occultation processing for NWP applications. In: Proceedings of the 20th EGU General Assembly. EGU 2018), Austria, 11329.

Xu, X.H., Liu, S.L., Luo, J., 2018. Analysis on the variation of global ABL top structure using COSMIC radio occultation refractivity. Geomatics Inf. Sci. Wuhan Univ. 43 (1), 94–100.

Zhran, M., Mousa, A., 2022. Planetary boundary layer height retrieval using GNSS Radio Occultation over Egypt. Egypt. J. Remote Sens. Space. Sci. 25 (2), 551–559.

Zhu, Z.Z., Xu, X.H., Luo, J., 2021. Inversion and analysis of Atmospheric Boundary Layer height using FY-3C radio occultation refractive index data. Geomatics Inf. Sci. Wuhan Univ. 46 (3), 395–401.